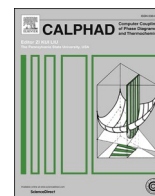




Contents lists available at ScienceDirect

Calphad

journal homepage: www.elsevier.com/locate/calphad

Thermodynamic re-modelling of the Cu–Nb–Sn system: Integrating the nausite phase

Jonas Lachmann^a, Mario J. Kriegel^a, Andreas Leineweber^{a,*}, Shun-Li Shang^b, Zi-Kui Liu^b

^a Institute of Materials Science, TU Bergakademie Freiberg, Gustav-Zeuner-Straße 5, 09599, Freiberg, Germany

^b Department of Materials Science and Engineering, The Pennsylvania State University, University Park, PA, 16802, USA

ARTICLE INFO

Keywords:
CALPHAD
nausite
Nb₃Sn
Cu–Nb–Sn
First-principles calculations

ABSTRACT

Currently available Cu–Nb–Sn phase diagrams lack the recently discovered nausite phase (Cu,Nb)Sn₂, which is an important intermediate in the course of thermal processing of superconducting Nb₃Sn wires. Processing decisively determines the resulting microstructure of Nb₃Sn and, thus, its superconducting properties. Lack of suitable and complete phase diagrams, however, obstructs rational design of such thermal processing procedures. To close this gap and to obtain valid knowledge of homogeneity and stability range of nausite, various Cu–Nb–Sn samples, which are heat-treated between 300 °C and 500 °C, are investigated. By means of energy-dispersive X-ray spectroscopy (EDX), a temperature-dependent homogeneity range of nausite is observed, which covers average mole fractions of Cu between 0.09 and 0.15. This is correlated with a change in the mean atomic volume and can be seen in the lattice parameters determined by X-ray diffraction (XRD). Additionally performed first-principles calculations on different CuSn₂ and NbSn₂ model structures confirm this trend. Furthermore, the peritectic decomposition of nausite to NbSn₂ and liquid at 586 °C is determined by means of *in situ* XRD and differential scanning calorimetry (DSC). By using the CALPHAD (CALculation of PHase Diagrams) approach, all these findings are used to extend a previous thermodynamic description of the Cu–Nb–Sn system by including the nausite as an additional phase. With this noteworthy integration, the updated modelling of the Cu–Nb–Sn system can be used for optimizing the multistage heat-treatment steps during processing superconducting Nb₃Sn wires.

1. Introduction

The run for the next generation of particle colliders drives the search for materials that deliver superior superconducting properties to generate even higher magnetic fields [1]. Nb₃Sn in conductor wires is a superconductor with a great potential in its critical current density [2]. Superconducting Nb₃Sn wires are already scheduled for magnets for the *Large Hadron Collider* upgrade instead of the Nb–Ti wires previously used, and large-scale application is planned for the *Future Circular Collider (FCC)* of the *European Organization for Nuclear Research (CERN)* [3]. However, the superconducting properties like critical current density and critical magnetic field depend strongly on the microstructure of the Nb₃Sn. This microstructure is significantly affected by different intermetallic phases formed as intermediates during the multi-stage heat treatments. In detail, starting from composite billets containing mainly Cu, Nb, and Sn, Nb₃Sn is formed at the last stage of heat treatment.¹ Therefore, a comprehensive knowledge about the formation processes of

intermetallic phases in the Cu–Nb–Sn system is crucial to optimize the microstructure of Nb₃Sn and, hence, its superconducting properties, as required for use of Nb₃Sn-based conductor cables e.g. in the *FCC*. Fundamental basis for planning of processing is knowledge of phase stability in the Cu–Nb–Sn system. This can be conveniently derived from a thermodynamic description within the framework of the CALculation of PHase Diagrams (CALPHAD) method [4]. However, the only available thermodynamic modelling of the Cu–Nb–Sn system by Li et al., in 2009 [5] does not consider existence of the ternary “nausite” phase, which was first reported in 2001 [6].

During heat treatment of certain types of conductor wires to produce the superconducting Nb₃Sn, nausite forms during the intermediate heat-treatment stages and decomposes at higher temperatures before Nb₃Sn formation takes place [6–13]. This leads to disconnected and large-grain Nb₃Sn, which degrades its superconducting properties [14–17]. Still, nausite already formed can also promote Cu diffusion to the Sn source, which decreases the amount of unwanted melt developing during

* Corresponding author.

E-mail address: Andreas.Leineweber@iww.tu-freiberg.de (A. Leineweber).

¹ The presence of Cu and formation of Cu–Sn intermetallics, in particular, accelerate the interaction of Nb with Sn.

<https://doi.org/10.1016/j.calphad.2022.102409>

Received 4 October 2021; Received in revised form 14 February 2022; Accepted 15 February 2022

Available online 22 February 2022

0364-5916/© 2022 Elsevier Ltd. All rights reserved.

Table 1

Overview of the investigated samples. Four different layered setups are produced by physical vapour deposition (PVD). The Cu and Sn layer thicknesses of the ternary PVD samples correspond to Cu:Sn atomic ratios of 1.2, 0.6, and 0.4, respectively. Furthermore, one loose powder mixture and four pressed powder mixtures with different overall compositions are prepared.

Technique	Layer thicknesses/ composition			Pre-heat treatment		Main heat treatment	
	Nb	Cu	Sn	T (°C)	t (h)	T (°C)	t (h)
PVD	substrate	2.0 µm	4.0 µm	220	48	300, 400 or 500	168
	substrate	1.5 µm	5.5 µm	220	48	300, 400 or 500	168
	substrate	1.0 µm	6.0 µm	220	48	300, 400 or 500	168
	substrate	–	5.0 µm	–	–	500	168
loose powder mixture	25 at.%	8 at. %	67 at.%	–	–	500	336
pressed powder mixtures	10 at.%	23 at.%	67 at.%	–	–	400 or 500	336
	10 at.%	30 at.%	60 at.%	–	–	400 or 500	336
	10 at.%	40 at.%	50 at.%	–	–	400 or 500	336
	35 at.%	10 at.%	55 at.%	–	–	400 or 500	336

further heat-treatment steps [14,17,18]. Hence, availability of a thermodynamic description of the Cu–Nb–Sn system including the nausite phase is highly desirable for planning of heat-treatments of such superconducting Nb₃Sn wires.

Nausite has a NiMg₂-type crystal structure with Nb and Cu simultaneously occupying the Ni sites, as described previously by the formula (Nb_{0.75}Cu_{0.25})Sn₂ [7]. Its crystal structure is closely related to the CuMg₂-type structure of the binary NbSn₂. In a recent work it was shown that NbSn₂ and nausite crystallites can grow in similar morphologies, and that their distinction e.g. based on electron backscatter diffraction (EBSD) data requires special care [7,19]. However, homogeneity and stability range of nausite are known only to a limited extent [7,9,10].

In the present paper this gap is closed by compositional analyses of various nausite-containing samples. The experimental findings are complemented by first-principles calculations on binary model structures. After collection of these data, a previous Cu–Nb–Sn database [5] is updated including the nausite phase. Moreover, this 2nd generation² CALPHAD [4] database is slightly re-modelled in view of the present assessment of literature data. As a consequence, the extended ternary description of the Cu–Nb–Sn system can serve as a valuable basis for optimizing the heat treatment to process Nb₃Sn wires with excellent superconducting properties.

2. Methods

2.1. Sample production and treatment

In order to obtain a significant amount of the nausite phase, layered samples as well as powder mixtures are produced and heat-treated at temperatures between 300 °C and 500 °C. An overview of all produced samples is given in Table 1. The layered samples are prepared by means of physical vapour deposition (PVD). On top of polycrystalline Nb plates (Goodfellow, purity 99.9%), first Cu and then Sn are deposited (sputter targets from FHR Anlagenbau GmbH, purity 99.99%). Three sample series are produced, differing in the ratio of layer thicknesses,

² The term 2nd generation indicates that the thermodynamic functions are phenomenological and valid only down to room temperature (298 K).

corresponding to Cu:Sn atomic ratios of 1.2, 0.6, and 0.4. The first ratio corresponds to the atomic ratio of the Cu₆Sn₅ intermetallic, the other two correspondingly contain Sn in excess. The samples are pre-heat-treated at 220 °C for 48 h to form Cu₆Sn₅ in contact with the Nb substrate by consuming the complete Cu layer. The excess-Sn forms an additional layer on top, and the substrate remains largely inert. Formation of the Cu₆Sn₅ at the contact with the Nb substrate avoids major dewetting of the liquid phase (forming at higher temperatures) from the substrate. After the step at 220 °C, the samples are subjected to a main heat treatment at either 300, 400, or 500 °C for 7 days. For comparison a binary Nb–Sn sample is also produced and heat-treated at 500 °C.

The first powder mixture sample consists of 8 at.% Cu, 25 at.% Nb, and 67 at.% Sn, which corresponds to the formula (Nb_{0.75}Cu_{0.25})Sn₂ given for nausite in the literature [7]. It is prepared by mechanical mixing of Nb (*E. Wägener GmbH*, purity 99.95%, –450 mesh), Cu (*ECKA Granules Germany GmbH*, purity 99.9%, –450 mesh), and Sn (*Sigma-Aldrich*, purity 99.8%, –325 mesh) powder under argon atmosphere in a mortar for 30 min, applying only low pressures with the pestle. Afterwards, the mixed powder is filled into a graphite crucible, which is then heat-treated for 2 weeks at 500 °C. The resulting material is used for *in situ* X-ray diffraction (XRD) and differential scanning calorimetry (DSC) because of its preserved porous and brittle character, which can be ground easily to powder.

Powder mixtures corresponding to various overall compositions are further prepared primarily for scanning electron microscope (SEM) and XRD investigations. For this purpose, powders are mixed as mentioned before, and are pressed at 750 MPa into pellets, which are subsequently heat-treated for 2 weeks at 400 °C or 500 °C. The powder compositions are selected to be located in some of the three-phase regions involving nausite. However, due to the slow kinetics [20], none of the samples are in global equilibrium after finishing the heat treatment. Nevertheless, large amounts of nausite are formed, and the local equilibria at phase interface contain useful tie-line information for thermodynamic modelling, though they are often for metastable equilibria between two phases when the stable ones may not be formed.

All these samples are first sealed in fused silica under argon atmosphere, then heat-treated and subsequently quenched in ice water. In case of the PVD samples, the ampoule is broken during the quenching process. Afterwards, the samples are cut, and one part is embedded, ground and polished down to 0.04 µm. For SEM studies, samples are covered by vaporized carbon for ensuring electrical conductivity. In case of the PVD samples, the other part of the plate-shaped sample is used for XRD investigations in reflection geometry. For the powder mixture samples, the embedded part is also used for XRD investigations. It should be mentioned that some of these samples were already presented in a conference paper [21].

2.2. Sample analysis

The SEM used is a *JEOL JSM-7800F* operated at 20 kV and 35 nA. Imaging is done using backscattered electrons on cross-sections. Energy-dispersive X-ray spectroscopy (EDX) is employed to study the homogeneity range of nausite. Corresponding point measurements are performed using the *Octane Elite Super EDS System of EDAX*. Additionally, EBSD is employed for phase identification. This is essential for the distinction of nausite and NbSn₂, showing strong similarities in growth morphology [19]. The applied EBSD camera is an *EDAX Hikari Super Elite* with a 480 × 480 pixel resolution. The software used for pattern and EDX spectrum acquisition is *TEAM* [22] and for pattern analysis *TSL OIM Analysis* [23].

On selected samples, electron-probe micro analysis with wavelength-dispersive X-ray spectroscopy (WDX) is also performed to study the local phase equilibria of nausite. For that purpose, a *JEOL JXA-8230 SuperProbe* operated at 20 kV and 40 nA is used. Calibration is performed on pure element standards from *ASTIMEX*.

XRD analysis is carried out in reflection geometry to study the lattice

Table 2

Space group, structure prototype, Strukturbericht symbol, and lattice parameters of the analysed phases used for EBSD indexing and Rietveld/Pawley refinement, in the latter case as starting values.

Phase	Nb	Sn	NbSn ₂	nausite/(Nb _{0.75} Cu _{0.25})Sn ₂	Cu ₆ Sn ₅ ^a	Cu ₃ Sn ^b
Space group	$Im\bar{3}m$	$I4_1/amd$	$Fddd$	$P6_222$	$P6_3/mmc$	$P6_3/mmc$
Prototype	W	β -Sn	CuMg ₂	NiMg ₂	Ni ₂ In/NiAs	Mg
Strukturbericht symbol	A2	A5	C _b	C _a	B8 _{1/2}	A3
a [Å]	3.294	5.831	9.874	5.647	4.192	2.756
b [Å]			5.626			
c [Å]		3.181	19.116	14.130	5.037	4.335
Reference	[25]	[26]	[27]	[7]	[28]	[29]

^a Corresponding to the disordered η form of the Cu₆Sn₅ intermetallic, which might transform to long-range ordered variants upon insufficiently rapid cooling. Due to the relatively weak effect of the order phenomena on the diffraction patterns, it is not tried to distinguish between differently ordered states of the Cu₆Sn₅ intermetallic, knowledge of which is summarised in Ref. [30].

^b Often referred to as ε phase. For EBSD analysis a simplified hexagonal closed packed structure is used, which derives from the orthorhombic superstructure structure in Ref. [29]. This avoids the distinction of practically indistinguishable orientations due to only small orthorhombic distortions and weak superstructure bands. Note that at high temperatures, the bcc-based β and γ phases exist in the compositional region of the (ε -)Cu₃Sn phase.

Table 3

Results from structure relaxation (lattice parameters and volume V_0^*) and equation of state fitting (DFT energy E_0 , volume V_0 , bulk modulus B_0 and its pressure derivative B_0') for different CuSn₂ and NbSn₂ crystal structures, together with the employed k-points meshes and the number of atoms in the unit cell (shown in the parentheses) of each compound for first-principles calculations.

Structure	Number of k-points, number of atoms	Lattice parameters	V_0^* (Å ³ /atom)	E_0 (eV/atom)	V_0 (Å ³ /atom)	B_0 (GPa)	B_0'
$Fddd$ -CuSn ₂	5 × 3 × 2 (48)	a = 5.395 Å b = 9.692 Å c = 19.475 Å	21.215	-3.9872	21.585	63.6	3.65
$Fddd$ -NbSn ₂	6 × 4 × 2 (48)	a = 5.709 Å b = 9.907 Å c = 19.287 Å	22.724	-6.1734	22.942	96.6	4.33
$P6_222$ -CuSn ₂	12 × 12 × 4 (18)	a = 5.512 Å c = 14.543 Å	21.256	-3.9861	21.542	63.4	5.66
$P6_222$ -NbSn ₂	14 × 14 × 5 (18)	a = 5.718 Å c = 14.441 Å	22.719	-6.1509	22.907	96.1	5.19
$I4/mcm$ -CuSn ₂	9 × 9 × 12 (12)	a = 6.829 Å c = 5.451 Å	21.184	-3.9971	21.504	63.6	5.58
$I4/mcm$ -NbSn ₂	11 × 11 × 13 (12)	a = 6.972 Å c = 5.591 Å	22.650	-6.1356	22.862	95.2	4.99

parameters of the crystal structures. For that purpose, a *D8 Advance* diffractometer of *Bruker* with Co-K α_1 radiation operated at 40 kV and 30 mA is used. *In situ* XRD is performed to study the decomposition of nausite. It is realized with another *D8 Advance* diffractometer with Cu-K α radiation operated at 40 kV and 40 mA, for which the sample is placed into an alumina crucible. The measurement is in the 2 θ -range from 29.5° to 35°, which contains significant peaks of Cu₆Sn₅, Sn, NbSn₂, and nausite. Thereby, a heating rate of 10 K/min, a step size of 0.02° and 0.25 s dwell per step are applied. The lattice parameters of nausite and NbSn₂ are determined using the *TOPAS* [24] software for Rietveld refinements or Pawley fits based on the measured XRD data. The crystallographic description of the observed phases for analysing EBSD patterns and values of lattice parameters serving as starting points for Rietveld refinement in XRD analysis can be found in [Table 2](#).

Transformation temperatures observed during DSC experiments are used to correct the temperatures recorded during the *in situ* XRD measurements on the same material. For that, the samples are placed in alumina crucibles and heated with a rate of 10 K/min in inert argon atmosphere using the *Netzsch Pegasus 404C* apparatus.

2.3. First-principles calculations

All first-principles calculations based on density functional theory (DFT) are performed by the Vienna Ab initio Simulation Package (VASP)

[31]. The ion-electron interaction is described by the projector augmented wave method [32] and the exchange-correlation functional is described by the generalized gradient approximation (GGA) developed by Perdew, Burke and Ernzerhof (PBE) [33]. The valence electron configurations considered are 4p⁶4d⁴5s¹ for Nb (i.e., the Nb_{pv} potential with a default cutoff energy ENMAX = 209 eV), 3p⁶4s²3d⁹ for Cu (i.e., the Cu_{pv} potential with ENMAX = 369 eV), and 4d¹⁰5s²5p² for Sn (i.e., the Sn_d potential with ENMAX = 241 eV). In the VASP calculations, the default plane wave cutoff energy defined by the setting of “PREC = Accurate” is employed for structural relaxations in terms of the Methfessel-Paxton method [34]. Final calculations of total energies are performed by the tetrahedron method with a Blöchl correction [35] using a fixed wave cutoff energy of 520 eV. The employed k-points meshes as well as the number of atoms in the unit cell of each model structure for first-principles calculations are given in [Table 3](#). The self-consistency of total energy is converged to at least 10⁻⁶ eV/atom.

Lattice parameters and fractional coordinates are reported for the as-relaxed VASP calculations (made available as crystallographic information files (CIF) in supplementary material). Taking the atomic volume V_0^* resulting from the as-relaxed lattice parameters, a series of further VASP calculations under the constraints of constant $V^{1/3} = 0.97, 0.98, \dots, 1.03 (V_0^*)^{1/3}$ are performed. For a given considered structure the parameters of a four-parameter Birch-Murnaghan (4BM) equation of state (EOS) as formulated in Ref. [36] are fitted, which can be written as:

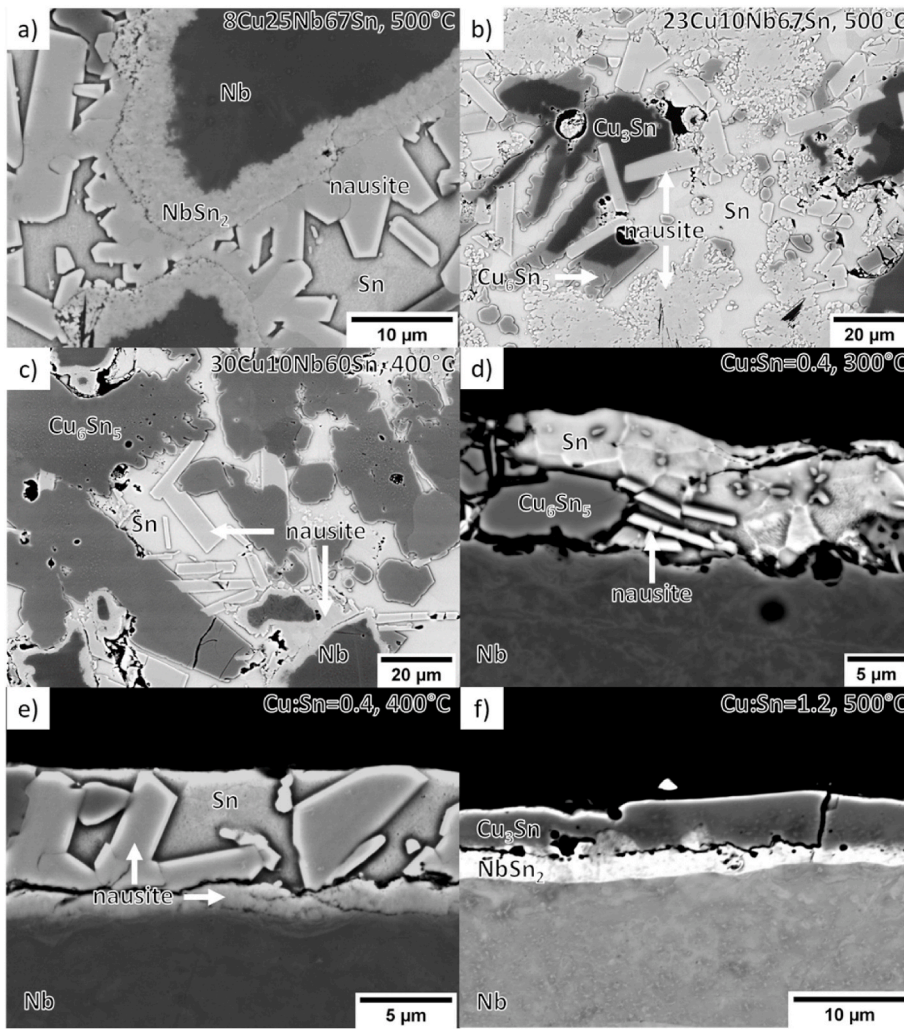


Fig. 1. SEM cross-sections of selected heat-treated powder mixture (a–c) and PVD samples (d–f) after heat treatment at the indicated temperatures (see also Table 1) revealing phase interfaces suggesting local phase equilibria of nausite with NbSn₂, Cu₆Sn₅, Cu₃Sn and liquid at the treatment temperature. In some cases, the nausite particles show faceted interfaces to the surrounding liquid, as was also mentioned in Ref. [19]. Although both phases appear with irregular interfaces, complementary analyses with EDX and EBSD clearly distinguish between NbSn₂ in (a) and nausite in (b). Cu₆Sn₅ in (b) was formed during cooling out of the supersaturated liquid after finishing the heat treatment. The basic elemental fractions of the powder mixtures respective the sample series of the PVD sample as well as the heat-treatment temperature is listed in every image.

$$E = E_0 + \frac{9}{16}V_0B_0 \left\{ (6 - B'_0) - (16 - 3B'_0) \left(\frac{V_0}{V}\right)^{\frac{2}{3}} + (14 - 3B'_0) \left(\frac{V_0}{V}\right)^{\frac{4}{3}} - (4 - B'_0) \left(\frac{V_0}{V}\right)^2 \right\}. \quad (1)$$

Thereby, the fitted parameters are the ground state E_0 , the volume V_0 , the bulk modulus B_0 as well as its pressure derivative B'_0 at a pressure of $P = 0$ GPa.

The first-principles calculations are performed for CuSn₂ and NbSn₂ in the structure types of CuMg₂ (*Fddd*, like found for pure NbSn₂; see Table 2), NiMg₂ (*P6₂22*, like found for nausite; see Table 2), and CuAl₂ (*I4/mcm*, Strukturbericht symbol C16). These model structures have been selected for consideration because of an observed sequence of crystal structures CuMg₂ (*Fddd*) → NiMg₂ (*P6₂22*) → CuAl₂ (*I4/mcm*) that are encountered for transition metal distannides with increasing (valence) electron number per atom [37]. As described in Ref. [7], the structure change starting from CuMg₂-type NbSn₂ into NiMg₂-type nausite can be understood due to the partial substitution of Nb by Cu, which increases the electron number. Although a CuAl₂-type phase (*I4/mcm*) appears to be absent in the Cu–Nb–Sn system, it is considered as model structure here for the sake of completeness. In the following,

these model structures for first-principles calculations are referred to as *Fddd*-NbSn₂, *P6₂22*-NbSn₂, *I4/mcm*-NbSn₂, *Fddd*-CuSn₂, *P6₂22*-CuSn₂, and *I4/mcm*-CuSn₂.

3. Literature review

The thermodynamic description of the Cu–Nb–Sn system reported by Li et al. [5] is the only available one for this system and is used as the basis for the present work. In their work several calculated isothermal sections of the Cu–Nb–Sn system for 675 °C and above are compared with experimental ones from the literature [38–42]. Agreement and disagreement with the experimental literature data were analysed there [5], and disagreement is convincingly attributed to inconsistent experimental data. As this temperature range is not in the focus of the present work and the associated data were accepted, an additional discussion is omitted here. Due to the fact that only ternary data at 660 °C and above were available [38–45] for consideration in Ref. [5], and because the nausite phase was apparently not known to the authors of that work, the

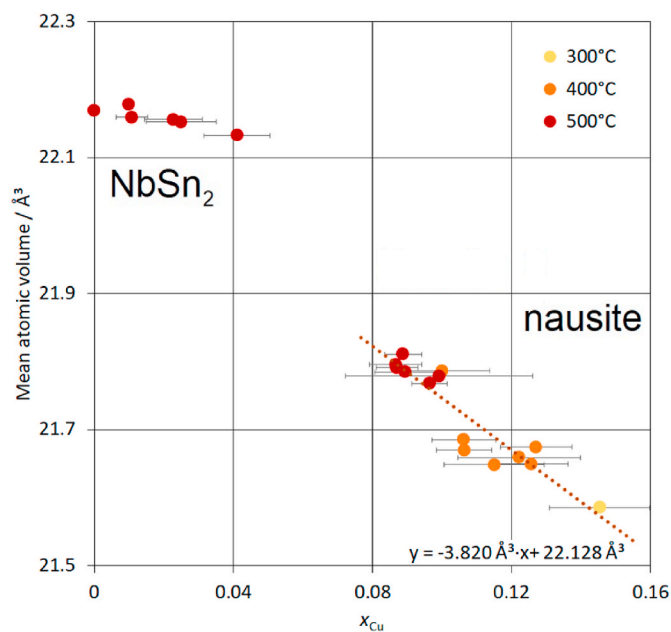


Fig. 2. Mean atomic volume versus molar fraction x_{Cu} measured in NbSn_2 and nausite in various samples ordered by heat treatment temperature. Each data point represents the outcome of XRD (volume) and EDX point measurements (composition) on one sample. Error bars mark the standard deviation of the EDX measurements of each sample. A linear fit of the nausite data, which serves as a comparison for the DFT data, is also displayed. Parts of the data have been already shown in a conference paper [21].

nausite phase was not modelled in that database.

Hence, it was first believed that it would be adequate to accept the thermodynamic modelling performed by Li et al. [5] as basis for integrating the new insights on nausite. However, a problem was encountered concerning the NbSn_2 phase. Li et al. [5] had introduced a binary solubility range that was explained by a better coincidence with the ternary homogeneity range of NbSn_2 found in the literature [41]. Admittedly, no specific measured data can be found there that would clearly indicate an off-stoichiometric Sn content. Other publications dealing with the ternary system neither deliver exact values that clearly suggest a Sn homogeneity range [38–40,43]. Hence, it was decided that a simplified stoichiometric description of the NbSn_2 phase would be more adequate. Therefore, the thermodynamic parameters for a stoichiometric NbSn_2 phase obtained in a previous binary description by Toffolon et al. [46] are adopted.

As it concerns the binary Cu–Sn system, some newer developments concerning A2/D0₃ high temperature phases [47] (bcc_A2/gamma in Ref. [5] and β/γ in footnote b of Table 2) and the Cu_6Sn_5 intermetallic [48] are not considered in the present work as it is believed that this insight is not relevant for processing of superconducting Nb_3Sn wires.

It is known from heat-treated superconducting Nb_3Sn wires that nausite shows local phase equilibria with NbSn_2 , Cu_6Sn_5 , Cu_3Sn , and Sn [9,14–18]. As mentioned above, the CuMg_2 -type NbSn_2 and NiMg_2 -type nausite both share a MSn_2 formula ($M = \text{Cu}, \text{Nb}$) with nausite being present at a significant substitution of Nb by Cu [7]. However, no systematic information on the homogeneity range of the nausite is available, although the formula $(\text{Nb}_{0.75}\text{Cu}_{0.25})\text{Sn}_2$ has been given in Ref. [7] in view of composition values from Ref. [10]. A previous work [19] has analysed the structural relation of nausite and NbSn_2 in detail, but did not discuss the homogeneity ranges. Additionally, it was observed that nausite disappears at $\sim 560^\circ\text{C}$ [9] in reacting conductor wires.

4. Evaluation of theoretical and experimental results

4.1. First-principles calculations

The results of the EOS fitting of the DFT-based first-principles calculations on the six binary model structures are listed in Table 3. The energy E_0 values indicate that for NbSn_2 the *Fddd* model structure is the most stable form, in agreement with the experimentally observed crystal structure [27]. In case of the hypothetical CuSn_2 , the lowest E_0 value occurs for the *I4/mcm* model structure. This finding agrees well with the predicted and observed stabilization of this structure as compared to the *Fddd* and *P6₂22* structures with increasing electron number in transition metal distannides [37].

4.2. Experimental results

4.2.1. Formation and phase equilibria of nausite

Exemplary SEM cross-sectional images of powder mixture and PVD samples treated at 300–500 °C are shown in Fig. 1. Supplementary use of EDX and EBSD analyses reveals the phases formed. Large amounts of nausite are visible, which appears mainly with faceted interfaces (a–e), but also irregular interfaces (b) or as a layer on the Nb substrate (e). EBSD analysis shows that the parallel surface traces of the faceted interfaces correspond to {001} planes, as already described in Ref. [19]. From observations of the corresponding phase interfaces, it can, furthermore, be concluded that nausite shows stable local two-phase equilibria with NbSn_2 , Cu_6Sn_5 , Cu_3Sn , and liquid³ at the respective treatment temperature.

Additionally, the PVD samples reveal increasing amounts of nausite with increasing Sn content in the samples. E.g. at 300 °C, the formed nausite plates are larger at a Cu:Sn ratio of 0.4 (Fig. 1d) than at a Cu:Sn ratio of 1.2. This can be explained by the fact that at Cu:Sn atomic ratios below the value of 1.2 (which corresponds to Cu_6Sn_5), residual Sn-rich liquid exists in between the Cu_6Sn_5 particles and is, therefore, in contact with the Nb substrate. Thus, Nb is carried through the liquid via diffusion or convection to the place of reaction where the Sn-rich nausite can be formed. At 500 °C nausite appears only at a Cu:Sn ratio of 0.4 together with NbSn_2 , while at lower Sn amounts NbSn_2 is present as the only Nb-containing intermetallic phase.

In case of the powder mixtures, nausite can be found in all samples. In contrast, NbSn_2 is only present at 500 °C and exhibits local phase equilibria with Cu_3Sn (Fig. 1f) and nausite (Fig. 1a).

It has to be mentioned that the phase interfaces of nausite or NbSn_2 to Nb unlikely result from a thermodynamic phase equilibrium, but from poor kinetics of the formation of Nb_3Sn [49].⁴ Nb_3Sn is not present in our investigated samples because its formation starts at around 600 °C, which is one typical heat treatment step during wire processing [14].

4.2.2. Homogeneity range of nausite

From the variety of samples containing NbSn_2 and/or nausite, XRD and EDX analyses yield lattice parameters and average mole fractions of Cu (x_{Cu}) of both phases. More precisely, average x_{Cu} values are calculated from a multitude of EDX data points of a given sample. As already mentioned, NbSn_2 and nausite belong to different, but structurally related crystal structures (see Table 2). Their chemical compositions differ due to partial substitution of Nb by Cu on one sublattice [7,19], while according to the sublattice model $x_{\text{Sn}} = 2/3$ for both phases. To

³ The liquid at treatment temperature is solidified at ambient temperature and mainly consists of Sn with limited amounts of dissolved Cu (or finely precipitated as Cu_6Sn_5), simplified named “Sn” in the whole work.

⁴ It cannot be excluded that local equilibrium develops in form of unresolved thin interlayers and/or in spike-like concentration profiles on a very narrow length scale [50,51]. In any case, the information from these interfaces with Nb cannot be exploited for the following evaluations.

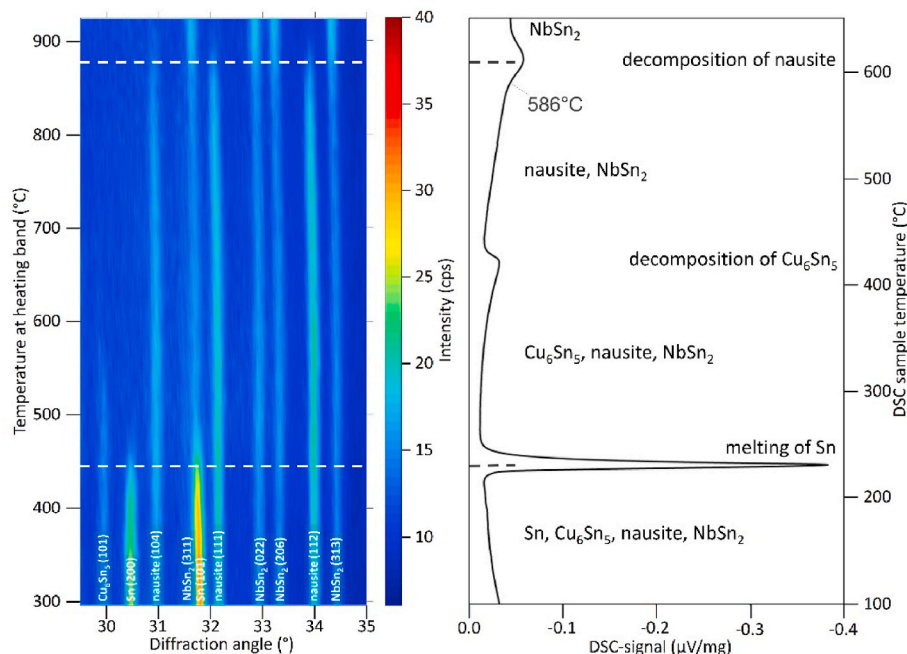


Fig. 3. *In situ* XRD (left) and DSC (right) measurements of a heat-treated powder mixture, showing the melting of Sn, the decomposition of Cu_6Sn_5 and finally the decomposition of nausite at 586°C . This is indicated also by naming the phases still present in the respective temperature range in the DSC diagram. Both diagrams are aligned in a way that the Sn melting and the decomposition of nausite are on the same level. Due to an incorrect temperature measurement for the *in situ* XRD, the temperature values of the phase reactions can be correlated with the temperature axis of the DSC measurement only. These data have been already shown in a conference paper [21] and were adopted from there.

compare the crystallographic data of NbSn_2 and nausite, the mean atomic volumes of these phases are calculated by dividing the respective unit-cell volume by the number of atoms in the unit cell. The corresponding values for each sample are plotted in Fig. 2 versus the x_{Cu} values determined for the respective phase.

Firstly, the range in x_{Cu} observed for the respective phase shows that both NbSn_2 and nausite exhibit a Cu homogeneity range. NbSn_2 can have a value of x_{Cu} up to approximately 0.04, and nausite shows x_{Cu} approximately from 0.09 to 0.15. Therefore, the chemical formula of nausite ($\text{Nb}_{0.75}\text{Cu}_{0.25}\text{Sn}_2$) formerly proposed [7] can be better expressed by the more general one $(\text{Cu},\text{Nb})\text{Sn}_2$. Secondly, the mean atomic volume and x_{Cu} in the respective phase are clearly correlated. The substitution of Nb by Cu leads to a reduction of the mean atomic volume. This is not surprising due to the smaller atomic radius of Cu in comparison with Nb and the fact that Cu substitutes Nb. Thirdly, as evident from Fig. 2, the mean Cu contents measured for nausite decrease with increasing temperature. This implies a correspondingly temperature-dependent homogeneity range of nausite.

Thereby, as mentioned above, it has been assumed that $x_{\text{Sn}} = 2/3$, implying no substitution of the Sn sites. In that case $x_{\text{Cu}} + x_{\text{Nb}} = 1/3$, and a higher Cu content is exactly coupled to a lower Nb content. However, EDX as well as WDX show some deviations in the measured x_{Sn} . It ranges from 0.64 to 0.69, but mostly $x_{\text{Sn}} > 2/3$ has been found. On the one side, this observation may originate from fluorescence excited in adjacent phases due to small size of the nausite and NbSn_2 particles. On the other side, inaccurate spectrum evaluation and standard calibration may cause systematic variations in the Sn content. As the structural model of both phases does not consider an occupation of Sn on Cu/Nb sites and vice versa, these deviations are neglected. In any case, the variation in the Cu content of the nausite phase at x_{Sn} of $2/3$ is more pronounced than the variation in the Sn content perpendicular to it.

As already mentioned, it is assumed that the observed variation in the mean atomic volume of nausite is caused by substitution of Nb by Cu, which is described by Zen's law [52]. To support this view, the evolution of the measured mean atomic volume with x_{Cu} of nausite can be compared with results of the first-principles calculations. $\text{P6}_222\text{-NbSn}_2$ and $\text{P6}_222\text{-CuSn}_2$ can be regarded here as end-members of the nausite solid solution, $(\text{Cu},\text{Nb})\text{Sn}_2$. The first-principles calculations predict the volume change expected upon substituting Nb by Cu in the respective

solution, in a similar way as predicted in the previous works for Cu_6Sn_5 intermetallic [48] and cementite [53].⁵ The values of the mean atomic volumes from the first-principles calculations can be found in Table 3. By considering the different Cu contents in the end-member structures, the volume change over the whole compositional range amounts to

$$\frac{\Delta V_0^{\text{P6}_222}}{\Delta x_{\text{Cu}}} = \frac{V_0^{\text{CuSn}_2} - V_0^{\text{NbSn}_2}}{x_{\text{Cu}}^{\text{CuSn}_2} - x_{\text{Cu}}^{\text{NbSn}_2}} = \frac{(21.542 - 22.907) \text{ \AA}^3}{\left(\frac{1}{3} - 0\right)} = -4.093 \text{ \AA}^3. \quad (2)$$

Linear fitting of the x_{Cu} -dependent experimental mean atomic volumes of nausite from Fig. 2 yields a slope of $-3.8 \pm 0.4 \text{ \AA}^3$. This value agrees well with the value obtained from Equation (2) in view of the error margins. This agreement confirms adequacy of the substitutional model and confirms the reliability of the EDX data determined for the nausite. Moreover, the derived conclusions on the homogeneity range of the nausite are supported.

4.2.3. Decomposition of nausite

XRD and SEM analyses of the powder mixture consisting of 8 at.% Cu, 25 at.% Nb, and 67 at.% Sn, reveal a significant phase fraction of nausite. The sample, moreover, contains NbSn_2 , Cu_6Sn_5 , solidified Sn, and residual Nb. Therefore, this sample is chosen for *in situ* XRD in combination with DSC analysis to investigate the decomposition of nausite at elevated temperatures. Both techniques are used complementarily because of the utilized *in situ* XRD setup. There, the thermocouple is in contact with the heating band and not with the sample itself. Therefore, the temperature at the sample position may differ. Hence, DSC measurements are performed to obtain reliable temperature information. *In situ* XRD is executed to relate the heat effects occurring in the DSC upon heating with information regarding occurring phase transformations. The results of these measurements are illustrated in Fig. 3.

⁵ Note that the absolute lattice parameters/mean atomic volumes predicted by first-principles calculations can easily differ in the order of 1% from the experimental values [54]. This is a significant deviation in view of the composition dependent variations. However, it is expected that the change of the lattice parameters upon changing composition is affected to a much lesser degree than the absolute values.

Table 4

Phase equilibria with nausite and the corresponding phase compositions found in the powder samples and determined by WDX that are used in the present modelling.

Temperature (°C)	Phase equilibrium	Phase composition (at.%)		
		Cu	Nb	Sn
400	nausite	11.5	20.0	68.5
	Cu ₆ Sn ₅	51.4	0.1	48.5
500	nausite	6.9	25.0	68.1
	NbSn ₂	3.8	28.0	68.2
	nausite	7.9	23.8	68.3
	Cu ₃ Sn	72.5	0.1	27.4

Three different reactions take place, starting with the melting of the residual Sn in the alloy, which corresponds to the strongest peak in the DSC curve. Further heating leads to the decomposition of Cu₆Sn₅ slightly above 400 °C. At 586 °C a further heat effect appears in the DSC measurement, which corresponds to the nausite decomposition in *in situ* XRD. Furthermore, the intensity of the peaks of NbSn₂ increases, which indicates the formation of NbSn₂ from the decomposed nausite. In another work [9], *in situ* synchrotron diffraction on an *Internal Tin* strand revealed the disappearance of reflections attributed to a ternary phase at about 560 °C. These reflections were later shown [7] to be attributable to nausite. Hence, the disappearance of the nausite in Ref. [9] in a reacting wire occurs at a relatively similar temperature, which is observed now under close-to-equilibrium conditions.

5. Thermodynamic modelling

5.1. Modelling of nausite and NbSn₂

The Gibbs energy functions of the pure elements are adopted from Dinsdale [55]. As a starting point, thermodynamic descriptions of the phases from the Cu–Nb–Sn system from Li et al. [5] are used. In this database, NbSn₂ is modelled using the compound energy formalism [56] with a sublattice model corresponding to (Cu,Nb,Sn)(Nb,Sn)₂. This allows the formation of a homogeneity range in the binary Nb–Sn and its extension in the ternary system. However, as described in Section 3, there is not sufficient data available in the literature supporting such a Sn solubility, which would provide information for the model used in Ref. [5].

Furthermore, the previous description of the ternary Cu–Nb–Sn system [5] does not contain the nausite phase due to lack of experimental data. Because of its structural relation to NbSn₂, the same model is applied now for nausite. Therefore, NbSn₂ and nausite are described here with the two-sublattice model (Cu,Nb)₁Sn₂. Their molar Gibbs energies G_m^θ ($\theta = \text{NbSn}_2, \text{nausite}$) are described with

$$G_m^\theta = G_m^{\theta,\text{srf}} + G_m^{\theta,\text{conf}} + G_m^{\theta,E} = y_{\text{Cu}} G_{\text{Cu:Sn}}^\theta + y_{\text{Nb}} G_{\text{Nb:Sn}}^\theta + RT(y_{\text{Cu}} \ln y_{\text{Cu}} + y_{\text{Nb}} \ln y_{\text{Nb}}) + G_m^{\theta,E}, \quad (3)$$

with y_{Cu} and y_{Nb} being the site fractions on the first, non-Sn sublattice. $G_m^{\theta,\text{srf}}$ represents the surface of reference defined by the endmembers Cu:Sn ($\theta = \text{CuSn}_2$) and Nb:Sn ($\theta = \text{NbSn}_2$). $G_m^{\theta,\text{conf}}$ is the contribution to the Gibbs energy from the configurational entropy of mixing and $G_m^{\theta,E}$ the excess Gibbs energy. The latter one is described by a third-order of Redlich-Kister polynomials expression [57].

$$G_m^{\theta,E} = y_{\text{Cu}} y_{\text{Nb}} \left({}^0L_{\text{Cu,Nb:Sn}}^\theta + (y_{\text{Cu}} - y_{\text{Nb}}) {}^1L_{\text{Cu,Nb:Sn}}^\theta + (y_{\text{Cu}} - y_{\text{Nb}})^2 {}^2L_{\text{Cu,Nb:Sn}}^\theta \right) \quad (4)$$

Table 5

Summary of the thermodynamic parameters of nausite, NbSn₂ and Nb₆Sn₅ in the Cu–Nb–Sn system. Nausite is added all-new, whereas the parameters of NbSn₂ and Nb₆Sn₅ are taken from existing databases and, if necessary, slightly adjusted. The parameters of all other phases of the Cu–Nb–Sn system can be found in the already existing database [5]. The whole updated database is provided as supplementary material.

Phase	Parameter	Function [J·mol ⁻¹ , J·mol ⁻¹ ·K ⁻¹]	Reference
nausite: (Cu,Nb) ₁ Sn ₂	${}^0G_{\text{Cu:Sn}}^{\text{nausite}}$	$GHSER_{\text{Cu}} + 2 \cdot GHSER_{\text{Sn}} + 63422.3 + 77.3 \cdot T$	This work
	${}^0G_{\text{Nb:Sn}}^{\text{nausite}}$	$GHSER_{\text{Nb}} + 2 \cdot GHSER_{\text{Sn}} - 39982.8 + 11.3 \cdot T$	This work
	${}^0L_{\text{Cu,Nb:Sn}}^{\text{nausite}}$	$-349959.0 + 102.5 \cdot T$	This work
	${}^1L_{\text{Cu,Nb:Sn}}^{\text{nausite}}$	$-6.0 - 8.1 \cdot T$	This work
	${}^2L_{\text{Cu,Nb:Sn}}^{\text{nausite}}$	$31.6 + 30.6 \cdot T$	This work
NbSn ₂ : (Cu,Nb) ₁ Sn ₂	${}^0G_{\text{Cu:Sn}}^{\text{NbSn}_2}$	$GHSER_{\text{Cu}} + 2 \cdot GHSER_{\text{Sn}} + 63091.1 + 77.3 \cdot T$	[5]
	${}^0G_{\text{Nb:Sn}}^{\text{NbSn}_2}$	$GHSER_{\text{Nb}} + 2 \cdot GHSER_{\text{Sn}} - 46487.0 + 11.3 \cdot T$	[46]
	${}^0L_{\text{Cu,Nb:Sn}}^{\text{NbSn}_2}$	$-183164.8 + 76.2 \cdot T$	This work
	${}^1L_{\text{Cu,Nb:Sn}}^{\text{NbSn}_2}$	$247972.8 - 77.5 \cdot T$	This work
	${}^2L_{\text{Cu,Nb:Sn}}^{\text{NbSn}_2}$	$-21035.9 + 71.8 \cdot T$	This work
Nb ₆ Sn ₅ : (Cu, Nb) ₂₄ Sn ₁₆ (Nb,Sn) ₄	${}^0G_{\text{Cu:Sn:Nb}}^{\text{Nb}_6\text{Sn}_5}$	$24 \cdot GHSER_{\text{Cu}} + 16 \cdot GHSER_{\text{Sn}} + 4 \cdot GHSER_{\text{Nb}} + 220000.0$	[5]
	${}^0G_{\text{Nb:Sn:Nb}}^{\text{Nb}_6\text{Sn}_5}$	$28 \cdot GHSER_{\text{Nb}} + 16 \cdot GHSER_{\text{Sn}} + 200086.5$	[46]
	${}^0G_{\text{Cu:Sn:Sn}}^{\text{Nb}_6\text{Sn}_5}$	$24 \cdot GHSER_{\text{Cu}} + 20 \cdot GHSER_{\text{Sn}} + 3034350.0 + 260.8 \cdot T$	[5]
	${}^0G_{\text{Nb:Sn:Sn}}^{\text{Nb}_6\text{Sn}_5}$	$24 \cdot GHSER_{\text{Nb}} + 20 \cdot GHSER_{\text{Sn}} - 651845.7 + 81.0 \cdot T$	[46]
	${}^0L_{\text{Cu,Nb:Sn:Sn}}^{\text{Nb}_6\text{Sn}_5}$	$-3600869.8 + 53.8 \cdot T$	This work
	${}^1L_{\text{Cu,Nb:Sn:Sn}}^{\text{Nb}_6\text{Sn}_5}$	$594224.3 - 35.6 \cdot T$	This work
	${}^2L_{\text{Cu,Nb:Sn:Sn}}^{\text{Nb}_6\text{Sn}_5}$	$-324256.2 + 70.1 \cdot T$	[5]

with ${}^0L_{\text{Cu,Nb:Sn}}^\theta$, ${}^1L_{\text{Cu,Nb:Sn}}^\theta$ and ${}^2L_{\text{Cu,Nb:Sn}}^\theta$ being the 0th, 1st, and 2nd order interaction parameters, respectively. Note that all these Gibbs energies refer to one formula unit (f.u.) of (Cu,Nb)₁Sn₂. Even though nausite and NbSn₂ are described as ternary line compounds, respectively, the 0th, 1st, and also 2nd order interaction parameters are used in this modelling. This originates from a previous description of the ternary Cu–Nb–Sn system [5], in which NbSn₂ is modelled with three interaction parameters. Thus, the order of these parameters is kept for NbSn₂ and adopted for the structurally related nausite phase as well.

For NbSn₂, the binary Nb–Sn parameter $G_{\text{Nb:Sn}}^{\text{NbSn}_2}$ is taken from Toffolon et al. [46], who treated NbSn₂ as a line compound. For describing the ternary Cu solubility, the parameter $G_{\text{Cu:Sn}}^{\text{NbSn}_2}$ of the binary end-member

and the 0th, 1st, and 2nd order interaction parameters $L_{\text{Cu,Nb:Sn}}^{\text{NbSn}_2}$ are taken from Li et al. [5].

For nausite, the Gibbs energies of the NbSn₂ and CuSn₂ end-members are adopted from NbSn₂ including a distinct offset each, which is predicted from the first-principles calculations (see Table 3). For this, the Gibbs energy differences between *Fddd*-CuSn₂ and *P6₂22*-CuSn₂ as well as between *Fddd*-NbSn₂ and *P6₂22*-NbSn₂ are taken equal to the DFT energy differences. These values are converted into J/mol-f.u. As a result, the Gibbs energy of *P6₂22*-CuSn₂ is by 331.2 J/mol-f.u. higher than the Gibbs energy of *Fddd*-CuSn₂, while the Gibbs energy of *P6₂22*-NbSn₂ is by 6504.2 J/mol-f.u. higher than the Gibbs energy of

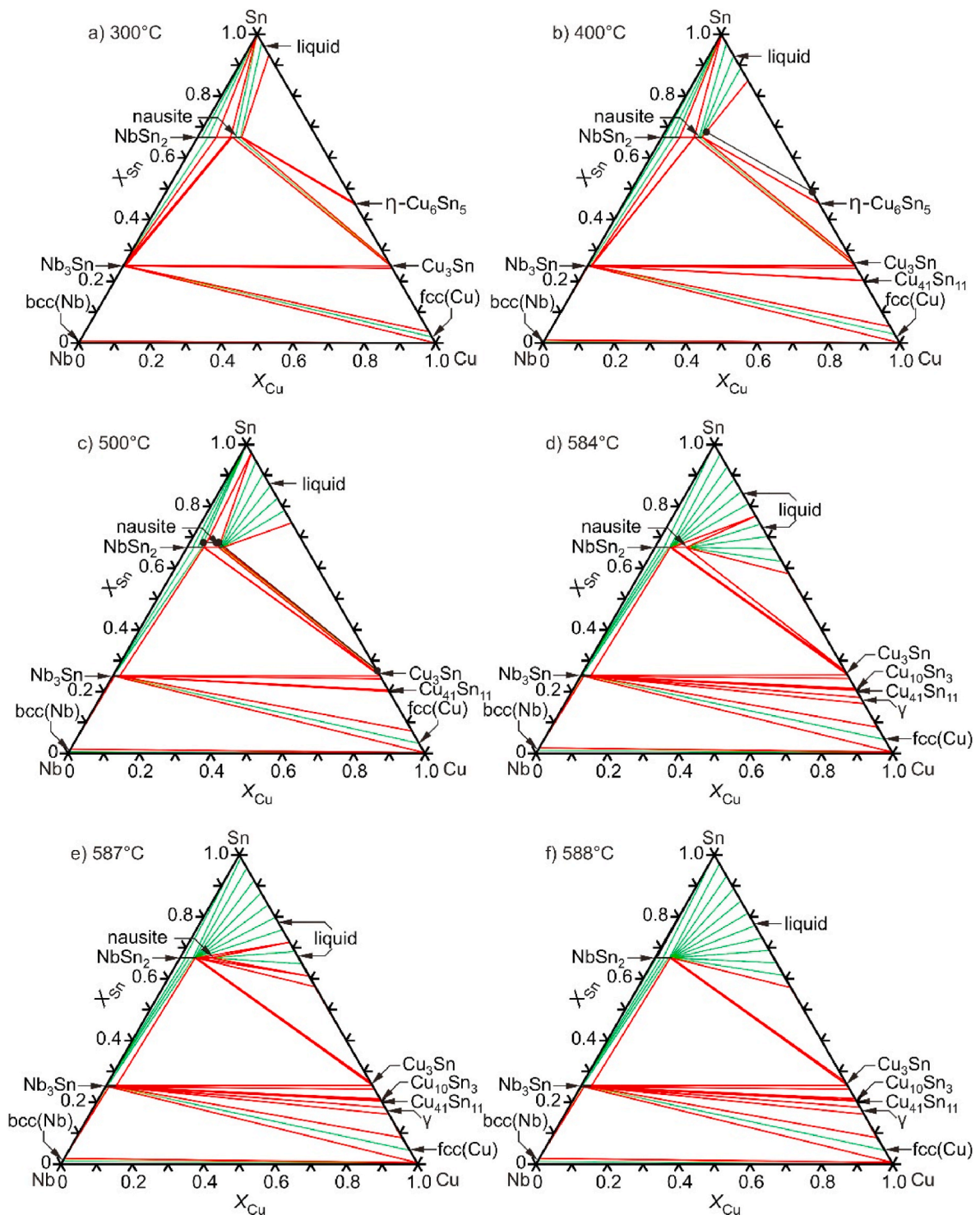


Fig. 4. Selected isothermal sections between 300 °C and 588 °C of the modelled Cu–Nb–Sn phase diagram. Parts of the data of a preliminary database containing variable Sn content NbSn₂ and nausite have been already shown in a conference paper [21]. Note that the liquid has such a small solubility for Nb that its region is practical confined to the Cu–Sn axis.

Fddd-NbSn₂.

These values are used as an offset to the binary parameters $G_{Cu:Sn}^{NbSn_2}$ and $G_{Nb:Sn}^{NbSn_2}$ to generate $G_{Cu:Sn}^{nausite}$ and $G_{Nb:Sn}^{nausite}$, which act as the binary end-members. To model the Gibbs energy of the ternary nausite phase, the three interaction parameters ${}^0L_{Cu,Nb:Sn}^{nausite}$, ${}^1L_{Cu,Nb:Sn}^{nausite}$, and ${}^2L_{Cu,Nb:Sn}^{nausite}$ are refined.

As they are the adjacent phases, which affect the phase equilibria

with nausite, the interaction parameters of NbSn₂ and Nb₆Sn₅ are slightly refined. The calculated phase equilibria above the decomposition temperature of nausite (e.g. Nb₆Sn₅ = Cu₃Sn + Nb₃Sn + NbSn₂, 599 °C) and the three-sublattice modelling of Nb₆Sn₅ are accepted from a previous modelling [5].

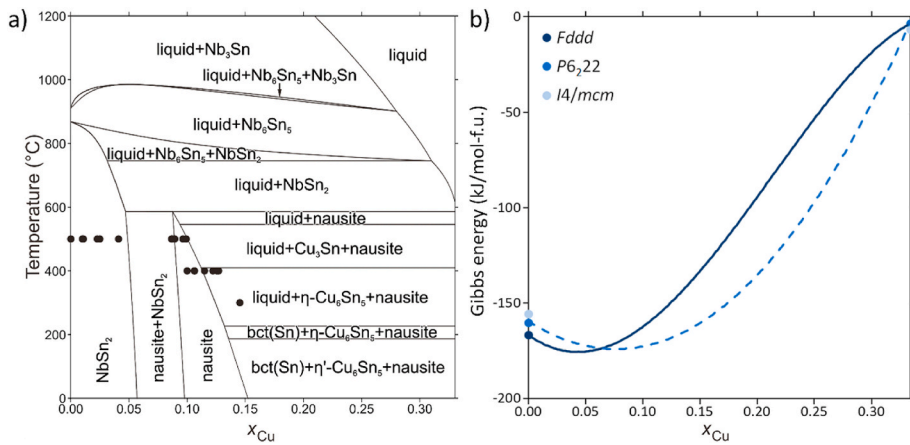


Fig. 5. Calculated isoplethal section (a) and Gibbs energy curves of NbSn₂ (solid line) and nausite (dashed line) phases at 500 °C (b) at $x_{\text{Sn}} = 2/3$ using the present database. In (a) a temperature-dependent homogeneity range of nausite is clearly visible. The EDX datapoints of the single-phase regions from Fig. 2 are shown as black circles. In (b) the results from the first-principles calculations are additionally shown as circles by using the calculated DFT energy differences for the different NbSn₂ and CuSn₂ crystal structures as an offset to the NbSn₂ Gibbs energy values at $x_{\text{Cu}} = 0$ respective $x_{\text{Cu}} = 1/3$.

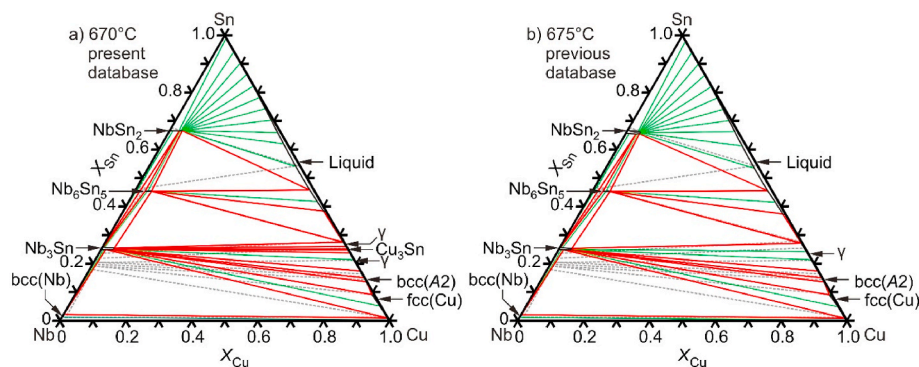


Fig. 6. Calculated isothermal sections of the Cu–Nb–Sn system at almost the same temperature using the present database (a) and the previous database from Li et al. [5]. They are compared to a published isothermal section inferred from experimental data at 675 °C from Neijmeijer and Kolster [38] coloured in grey.

Table 6

Calculated invariant reactions in the Cu–Nb–Sn system with nausite participating.

Reaction ^a	Temperature (°C)
liquid + NbSn ₂ = nausite	588
liquid + NbSn ₂ = Cu ₃ Sn + nausite	586
NbSn ₂ + Cu ₃ Sn = nausite + Nb ₃ Sn	410
liquid + Cu ₃ Sn = η - Cu ₆ Sn ₅ + nausite	410
liquid + NbSn ₂ = bct(Sn) + nausite ^b	232
liquid + nausite = bct(Sn) + η - Cu ₆ Sn ₅ ^b	226
Cu ₃ Sn + η - Cu ₆ Sn ₅ = η' - Cu ₆ Sn ₅ + nausite	189
η - Cu ₆ Sn ₅ = bct(Sn) + η' - Cu ₆ Sn ₅ + nausite ^b	186

^a Not considering newer developments concerning the Cu–Sn system [47,48] as mentioned in Section 3.

^b Note that β-Sn phase is named here and in Fig. 7 “bct(Sn)” as this is the same denotation in the previous ternary description of the Cu–Nb–Sn system [5].

5.2. Selected phase equilibria

For thermodynamic modelling, only the selected WDX data points of nausite and adjacent phases being in supposed local equilibrium are considered, using only data from powder samples (see Table 1). Equilibria with the liquid are not taken into account for the modelling procedure because of compositional changes in the liquid, which likely occur upon solidification. Due to that, high Cu contents in the liquid phase (as expected from the phase diagram) cannot be detected. The phase equilibria of nausite used in the present modelling are listed in Table 4.

Here, the already mentioned higher Sn content in nausite and NbSn₂ detected by WDX becomes visible. As this is also observed for Cu₆Sn₅

and Cu₃Sn here, this seems to be rather a systematic error of the measurement. Furthermore, as the structural model of (Cu,Nb)Sn₂ does not permit a Sn off-stoichiometry, this is not of significance here. The determined Sn content, which deviates up to 2 at.%, has an influence on the determined Cu- and Nb contents, which will then differ in the calculated phase equilibria. Therefore, an uncertainty up to 2 at.% regarding the Cu- and Nb contents in the modelling has to be considered.

Additionally, the results from *in situ* XRD and DSC measurements indicate that nausite decomposes at 586 °C to liquid and NbSn₂. The thermodynamic parameters are optimized in a way that nausite decomposes at ~586 °C in order to form the two-phase equilibrium of liquid + NbSn₂ at higher temperatures. Furthermore, to retain the phase equilibria at higher temperatures, different three- and four-phase equilibria with NbSn₂ and/or Nb₆Sn₅ as reported in the literature [38,40,41] are used in the optimization procedure. The optimization is carried out by using the PARROT module [4] of the Thermo-Calc Software [58]. Phase diagrams are calculated with the Thermo-Calc Software as well.

6. Discussion of the optimized thermodynamic description

An extract of the thermodynamic description of the Cu–Nb–Sn system can be found in Table 5, in which the model parameters of nausite, NbSn₂, and Nb₆Sn₅ are listed. The thermodynamic parameters for all other phases remain unchanged with respect to the previous database [5].

Calculated isothermal sections illustrating the phase equilibria with the nausite phase are shown in Fig. 4. Additionally, the experimental data from Table 4 are superimposed. A temperature-dependent variation of the homogeneity range of nausite is visible comparing the isothermal sections of 300 °C, 400 °C, and 500 °C. Moreover, this can be seen in the

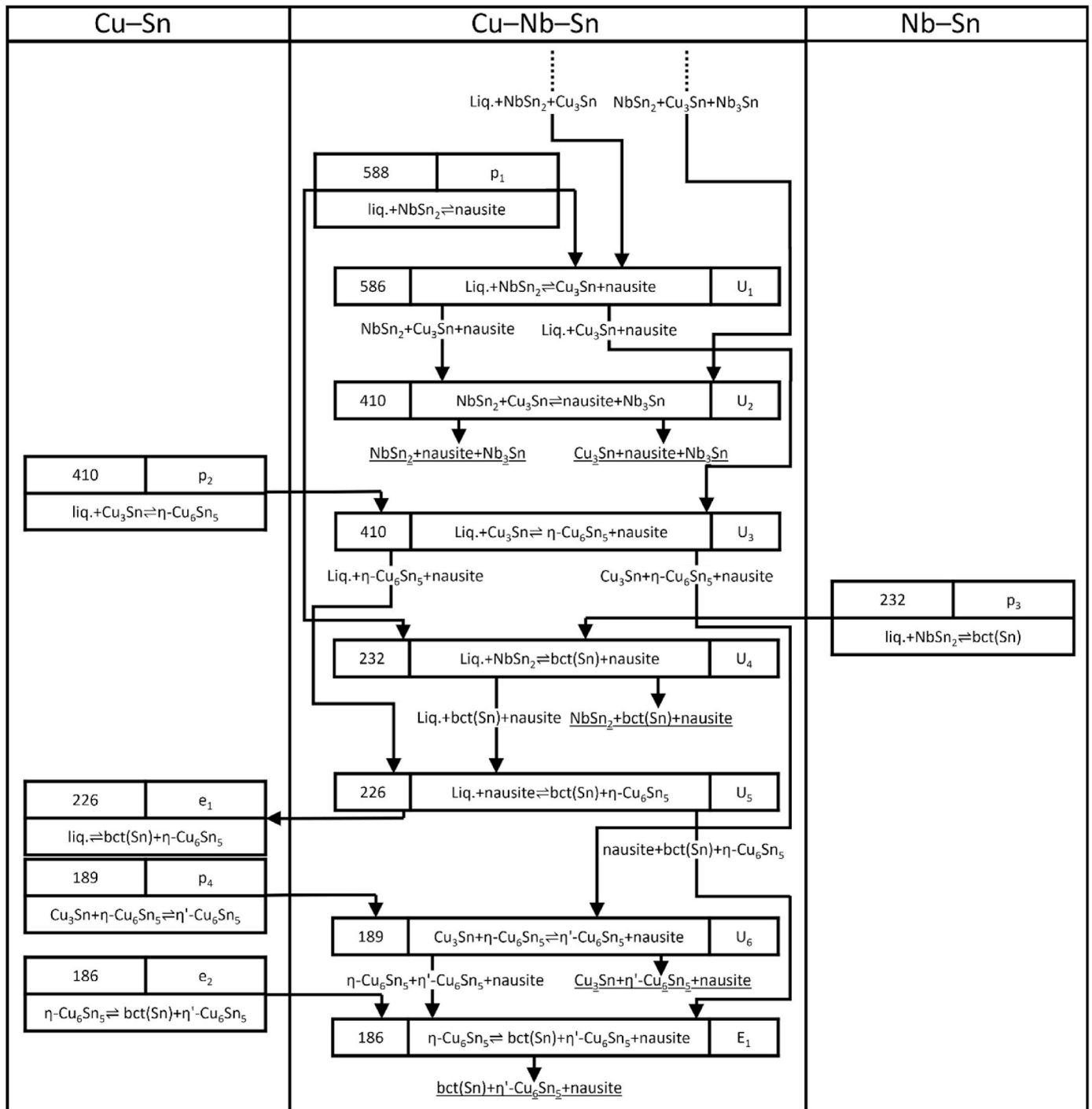


Fig. 7. Partial Scheil reaction scheme of the Cu-Nb-Sn system showing the phase equilibria and heterogeneous reactions of nausite. The reaction temperatures are given in degrees Celsius.

isoplethal section at $x_{Sn} = 2/3$ more clearly, which is illustrated in Fig. 5a. The EDX datapoints from Fig. 2 are also shown there. Admittedly, the temperature-dependent variation of the homogeneity range is smaller in the calculated phase diagram than implied by the EDX data. This was also recognized during the optimization procedure. However, a stronger temperature shift of the homogeneity range would require higher temperature dependencies of the interaction parameters. This would lead to incorrect phase equilibria at higher and lower temperatures. Hence, the values of the interaction parameters are kept preferably on a smaller level, which delivers sufficient results. Admittedly, only ${}^0L_{Cu,Nb:Sn}^{nausite}$ shows high values, which, however, result from high

values of ${}^0L_{Cu,Nb:Sn}^{NbSn_2}$ (see Table 5). Again, the latter ones are taken from Ref. [5] and adjusted only slightly to keep the modelled phase equilibria at higher temperatures.

Besides the temperature shift, also a continued widening of the homogeneity range of the nausite phase towards lower temperatures can be seen in Fig. 5a. At higher temperatures on the one side, this trend follows the course of the liquidus line. On the other side, the homogeneity range shows an unusual widening towards even lower temperatures. Unusual homogeneity ranges, however, were also reported for phases with crystal-structure selection due to electronic origin, like it is the case for Hume-Rothery phases [59]. In fact, it has been argued that

formation of the nausite structure is indeed determined by the electron per atom ratio (“valence electron concentration”) [7], as it had previously been worked out for a wide series of transition metal distannides ($M\text{Sn}_2$) [37].

Exemplarily calculated Gibbs energy curves of NbSn_2 and nausite at $x_{\text{Sn}} = 2/3$ and 500 °C are shown in Fig. 5b. The energy differences extracted from the first-principles calculations for the different NbSn_2 and CuSn_2 crystal structures (including the $I4/mcm$ - CuSn_2 and $-\text{NbSn}_2$ not considered in the course of CALPHAD modelling) are evident at $x_{\text{Cu}} = 0$ and $1/3$. It can be seen that at low x_{Cu} values NbSn_2 is the stable phase while nausite becomes stable at intermediate values of x_{Cu} .

Besides the temperature-dependent shift in the solubility range of nausite making up a few at.%, a change in the surrounding phase equilibria can be seen (Fig. 4b and c). At low temperatures, a two-phase region nausite + Nb_3Sn (which is not formed experimentally at these temperatures for kinetic reasons) is predicted adjoined to the two three-phase regions of NbSn_2 + nausite + Nb_3Sn and Cu_3Sn + nausite + Nb_3Sn . At 410 °C a U-type reaction $\text{NbSn}_2 + \text{Cu}_3\text{Sn} = \text{nausite} + \text{Nb}_3\text{Sn}$ takes place. This generates, above its invariant temperature, a two-phase region $\text{NbSn}_2 + \text{Cu}_3\text{Sn}$ with the adjoined three-phase regions $\text{NbSn}_2 + \text{Cu}_3\text{Sn} + \text{nausite}$ and $\text{NbSn}_2 + \text{Cu}_3\text{Sn} + \text{Nb}_3\text{Sn}$. This U-type reaction may be a reason that in the Cu-containing samples treated at 300 °C and 400 °C only nausite forms, whereby at 500 °C NbSn_2 appears. Thinking of the PVD samples, the diffusion path from Nb to Cu–Sn, therefore, requires the formation of NbSn_2 above the U-type reaction temperature. At lower temperatures, nausite can be formed without simultaneous formation of NbSn_2 . This was also already observed in heat-treated *Internal Tin* wires, where after a 400 °C heat treatment step nausite was found, but NbSn_2 when heat-treated at 450 °C [21]. The two-phase region $\text{NbSn}_2 + \text{Cu}_3\text{Sn}$, which exists above the U-type reaction temperature, agrees with the local phase equilibrium shown in Fig. 1f.

The isothermal sections of 584 °C, 587 °C, and 588 °C (Fig. 4d–f) consider the temperature range around the decomposition of nausite. At 586 °C the U-type reaction liquid + $\text{NbSn}_2 = \text{Cu}_3\text{Sn} + \text{nausite}$ takes place. At slightly higher temperatures, two different three-phase regions liquid + NbSn_2 + nausite are present with the two-phase regions NbSn_2 + nausite as well as liquid + nausite between them. At 588 °C nausite decomposes by a pseudo-binary peritectic reaction liquid + $\text{NbSn}_2 = \text{nausite}$, which is very close to 586 °C determined by DSC.

Above the decomposition temperature of nausite, comparable phase equilibria are predicted by the previous modelling from Li et al. [5] and the present one. The only deviation worth mentioning is encountered for 675 °C, where experimental data from Neijmeijer and Kolster [38] are available. The reason for this disagreement is the temperature of the U-type reaction liquid + $\text{Nb}_3\text{Sn} = \gamma + \text{Nb}_6\text{Sn}_5$. This reaction takes place at 670 °C according to the present database, which is slightly lower compared to the temperature calculated by Li et al. [5] (675 °C) and estimated by Neijmeijer and Kolster [38] (680 ± 4 °C). Thus, the phase equilibria in the isothermal section at 675 °C calculated by Li et al. [5] differ significantly to the phase equilibria calculated by the present database. However, these deviations become negligible when the calculated isothermal section at 675 °C using the database from Li et al. [5] is compared with the one using the present database at 670 °C. The latter temperature is chosen just below the temperature of the above-mentioned U-type reaction according to the present database; see Fig. 6 for the comparison. Similar deviations from the experimental isothermal section reported by Neijmeijer and Kolster [38] can be seen (with the only exception being the presence of the Cu_3Sn phase resulting from the binary system).

At higher temperatures, no significant differences appear in the determined phase equilibria using the present database compared to the previous one from Li et al. [5]. Therefore, only the predicted invariant reactions in the Cu–Nb–Sn system with nausite participating are listed in Table 6.

The corresponding partial Scheil reaction scheme [60] resulting from the present database is shown in Fig. 7, which begins with the formation

of nausite at 588 °C. This updates the reaction scheme reported by Li et al. [5] at lower temperatures, where no experimental data were available. The reactions at higher temperatures remain almost unchanged. It has to be mentioned that close sequences of invariant reactions, e.g., as determined near the decomposition of nausite, cannot be ensured to occur exactly in this way. Small changes in the thermodynamic functions may change these sequences significantly. Thus, the present database only offers one possible way to realize the decomposition of nausite via a set of invariant reactions.

7. Conclusions

This work presents the first detailed investigation of phase equilibria in the ternary Cu–Nb–Sn system involving the nausite phase, which is based on the analysis of various heat-treated ternary samples as well as first-principles calculations. A temperature-dependent homogeneity range of nausite could be observed, which shifts to lower Cu contents at higher temperatures. A correlation between Cu content and mean atomic volume was revealed by means of EDX and XRD, which was also confirmed by first-principles calculations on binary CuSn_2 and NbSn_2 model structures. Combined *in situ* XRD and DSC studies revealed a peritectic decomposition of nausite at 586 °C.

Based on these findings, a previous thermodynamic description of the Cu–Nb–Sn system was extended by the nausite phase. Thereby, the nausite was described by the same type of two-sublattice model ($\text{Cu, Nb}_1\text{Sn}_2$), which was also used for the structurally related NbSn_2 , implying a fixed molar fraction $x_{\text{Sn}} = 2/3$. Additionally, the interaction parameters of the adjacent NbSn_2 and Nb_6Sn_5 phases were only slightly adjusted as compared to a previous 2nd generation CALPHAD database.

The obtained thermodynamic description of the Cu–Nb–Sn system covers the experimentally determined homogeneity and stability range of nausite in a reasonable manner. Furthermore, the calculated phase equilibria at higher temperatures coincide almost completely with that ones calculated using a previous database. Therefore, this work yields the first complete description of the phase equilibria in the Cu–Nb–Sn system in the temperature range between 200 °C and 700 °C, which is relevant for adjusting the heat-treatment procedures in processing superconducting Nb_3Sn wires.

Data availability

All data included in this study are available upon request by contact with the corresponding author.

Declaration of competing interest

The authors declare that they have no known competing financial interests or personal relationships that could have appeared to influence the work reported in this paper.

Acknowledgements

The authors thank Dr.-Ing. Alexander Walnsch for fruitful discussions regarding the thermodynamic optimization as well as M.Sc. André Treichel and Dipl.-Ing. Martin Thümmeler for conducting the WDX and *in situ* XRD measurements. JL and AL acknowledge the financial support by the *European Organization for Nuclear Research (CERN)* within Collaboration Agreement KE3985. SLS and ZKL acknowledge the financial support by the *U.S. National Science Foundation (NSF)* with Grant No. CMMI-2050069. First-principles calculations were performed partially on the resources of the *National Energy Research Scientific Computing Center (NERSC)* supported by the *U.S. Department of Energy Office of Science User Facility* operated under Contract No. DE-AC02-05CH11231, and partially on the resources of the *Extreme Science and Engineering Discovery Environment (XSEDE)* supported by *NSF* with Grant No. ACI-1548562.

Appendix A. Supplementary data

Supplementary data to this article can be found online at <https://doi.org/10.1016/j.calphad.2022.102409>.

References

- [1] A. Paul, T. Laurila, V. Vuorinen, Microstructure, diffusion and growth mechanism of Nb₃Sn superconductor by bronze technique, in: Adir Luiz (Ed.), *Superconductor* (2010) 47–68.
- [2] A. Godeke, A review of the properties of Nb₃Sn and their variation with A15 composition, morphology and strain state, *Supercond. Sci. Technol.* 19 (2006) R68–R80, <https://doi.org/10.1088/0953-2048/19/8/R02>.
- [3] A. Ballarino, S.C. Hopkins, B. Bordini, D. Richter, D. Tommasini, L. Bottura, M. Benedikt, et al., The CERN FCC conductor development program: a worldwide effort for the future generation of high-field magnets, *IEEE Trans. Appl. Supercond.* 29 (2019) 1–9, <https://doi.org/10.1109/TASC.2019.2896469>.
- [4] H.L. Lukas, S.G. Fries, B. Sundman, *Computational Thermodynamics: the CALPHAD Method*, Cambridge University Press, Cambridge, 2007.
- [5] M. Li, Z. Du, C. Guo, C. Li, Thermodynamic optimization of the Cu–Sn and Cu–Nb–Sn systems, *J. Alloys Compd.* 477 (2009) 104–117, <https://doi.org/10.1016/j.jallcom.2008.09.141>.
- [6] M.T. Naus, P.J. Lee, D.C. Larbalestier, The influence of the starting Cu–Sn phase on the superconducting properties of subsequently reacted internal-Sn Nb₃Sn conductors, *IEEE Trans. Appl. Supercond.* 11 (2001) 3569–3572, <https://doi.org/10.1109/77.919835>.
- [7] S. Martin, A. Walnsch, G. Nolze, A. Leineweber, F. Léau, C. Scheuerlein, The crystal structure of (Nb_{0.75}Cu_{0.25})Sn₂ in the Cu–Nb–Sn system, *Intermetallics* 80 (2017) 16–21, <https://doi.org/10.1016/j.intermet.2016.09.008>.
- [8] C. Scheuerlein, M. Di Michiel, G. Arnau, R. Flükiger, F. Buta, I. Pong, L. Oberli, et al., Coarse Nb₃Sn grain formation and phase evolution during the reaction of a high Sn content internal tin strand, *IEEE Trans. Appl. Supercond.* 21 (2011) 2554–2558, <https://doi.org/10.1109/TASC.2010.2082476>.
- [9] C. Scheuerlein, M. Di Michiel, G. Arnau Izquierdo, F. Buta, Phase transformations during the reaction heat treatment of internal tin Nb₃Sn strands with high Sn content, *IEEE Trans. Appl. Supercond.* 18 (2008) 1754–1760, <https://doi.org/10.1109/TASC.2008.2006912>.
- [10] M. Cantoni, C. Scheuerlein, P.-Y. Pfirter, F. de Borman, J. Rossen, G. Arnau, L. Oberli, et al., Sn concentration gradients in Powder-in-Tube superconductors, *J. Phys. Conf. Ser.* 234 (2010) 22005, <https://doi.org/10.1088/1742-6596/234/2/022005>.
- [11] M. Di Michiel, C. Scheuerlein, Phase transformations during the reaction heat treatment of powder-in-tube Nb₃Sn superconductors, *Supercond. Sci. Technol.* 20 (2007) L55–L58, <https://doi.org/10.1088/0953-2048/20/10/L01>.
- [12] C. Segal, C. Tarantini, Z.H. Sung, P.J. Lee, B. Sailer, M. Thoener, K. Schlenga, et al., Evaluation of critical current density and residual resistance ratio limits in powder in tube Nb₃Sn conductors, *Supercond. Sci. Technol.* 29 (2016) 85003, <https://doi.org/10.1088/0953-2048/29/8/085003>.
- [13] X. Wu, X. Peng, M.D. Sumption, E. Gregory, M. Tomsic, E.W. Collings, Titanium diffusion and phase formation in tube-type rod-in-tube and internal-tin Nb₃Sn strands, *AIP Conf. Proc.* 824 (2006) 504–512, <https://doi.org/10.1063/1.2192388>.
- [14] M. Field, H. Miao, C. Sanabria, J. Parrell, Strand Critical Current Density in Nb₃Sn Superconducting Strands via a Novel Heat Treatment, US Patent, 2018, p. 212136.
- [15] I. Pong, L.-R. Oberli, L. Bottura, Cu diffusion in Nb₃Sn internal tin superconductors during heat treatment, *Supercond. Sci. Technol.* 26 (2013) 1–10, <https://doi.org/10.1088/0953-2048/26/10/105002>.
- [16] M. Naus, Optimization of Internal-Sn Nb₃Sn Composites, Dissertation. University of Wisconsin-Madison, 2002.
- [17] C. Sanabria, A New Understanding of the Heat Treatment of Nb–Sn Superconducting Wires, Dissertation. Florida State University, 2017.
- [18] C. Sanabria, P.J. Lee, D.C. Larbalestier, The vital role of a well-developed Sn–Nb–Cu membrane for high J_c RRP® Nb₃Sn wires, *Superconduct. News Forum.* 10 (2016) 1–2.
- [19] J. Lachmann, N. Huber, A. Leineweber, Nausite and NbSn₂ – growth and distinction of structural related intermetallic phases in the Cu–Nb–Sn system, *Mater. Char.* 168 (2020) 110563, <https://doi.org/10.1016/j.matchar.2020.110563>.
- [20] T. Studnitzky, R. Schmid-Fetzer, Phase formation and reaction kinetics in M–Sn systems (M= Zr, Hf, Nb, Ta, Mo), *Z. Metallkd.* 93 (2002) 894–903.
- [21] S.C. Hopkins, A. Baskys, A. Ballarino, J. Lachmann, A. Leineweber, Phase evolution during heat treatment of Nb₃Sn wires under development for the FCC study, *IEEE Trans. Appl. Supercond.* 31 (2021) 1–6, <https://doi.org/10.1109/TASC.2021.3063675>.
- [22] EDAX, TEAM V4.5, Mahwah, United States of America.
- [23] EDAX, TSL OIM Analysis V8, Mahwah, United States of America.
- [24] A.X.S. Bruker, V.4 TOPAS, General Profile and Structure Analysis Software for Powder Diffraction Data, User's Manual, Bruker AXS, Karlsruhe, Germany, 2008.
- [25] M.C. Neuburger, Präzisionsmessung der Gitterkonstante von sehr reinem Niob, *Z. Kristallogr., Kristallgeo. Kristallphy. Kristallchem.* 93 (1936) 158–159.
- [26] E.R. Jette, F. Foote, Precision determination of lattice constants, *J. Chem. Phys.* 3 (1935) 605–616, <https://doi.org/10.1063/1.1749562>.
- [27] T. Wölpel, W. Jeitschko, Crystal structures of VSn₂, NbSn₂ and CrSn₂ with Mg₂Cu-type structure and NbSnSb with CuAl₂-type structure, *J. Alloys Compd.* 210 (1994) 185–190, [https://doi.org/10.1016/0925-8388\(94\)90136-8](https://doi.org/10.1016/0925-8388(94)90136-8).
- [28] A. Gangulee, G.C. Das, M.B. Bever, An X-ray diffraction and calorimetric investigation of the compound Cu₆Sn₅, *Metall. Trans. A* 4 (1973) 2063–2066, <https://doi.org/10.1007/BF02643268>.
- [29] H. Knödler, Der strukturelle Zusammenhang zwischen gamma- und epsilon-Phase im System Kupfer-Zinn, *Acta Crystallogr.* 10 (1957) 86–87, <https://doi.org/10.1107/S0365110X57000225>.
- [30] A. Leineweber, C. Wieser, W. Hügel, Crystal structure of incommensurate η'-Cu_{1.235}Sn intermetallic, *Z. für Kristallogr. - Cryst. Mater.* 235 (2020) 445–457, <https://doi.org/10.1515/zkri-2020-0055>.
- [31] G. Kresse, J. Furthmüller, Efficient iterative schemes for ab initio total-energy calculations using a plane-wave basis set, *Phys. Rev. B* 54 (1996) 11169–11186, <https://doi.org/10.1103/PhysRevB.54.11169>.
- [32] G. Kresse, D. Joubert, From ultrasoft pseudopotentials to the projector augmented-wave method, *Phys. Rev. B* 59 (1999) 1758–1775, <https://doi.org/10.1103/PhysRevB.59.1758>.
- [33] J.P. Perdew, K. Burke, M. Ernzerhof, Generalized gradient approximation made simple, *Phys. Rev. Lett.* 77 (1996) 3865–3868, <https://doi.org/10.1103/PhysRevLett.77.3865>.
- [34] M. Methfessel, A.T. Paxton, High-precision sampling for Brillouin-zone integration in metals, *Phys. Rev. B* 40 (1989) 3616–3621, <https://doi.org/10.1103/PhysRevB.40.3616>.
- [35] P.E. Blöchl, O. Jepsen, O.K. Andersen, Improved tetrahedron method for Brillouin-zone integrations, *Phys. Rev. B* 49 (1994) 16223, <https://doi.org/10.1103/PhysRevB.49.16223>.
- [36] S.-L. Shang, Y. Wang, D. Kim, Z.-K. Liu, First-principles thermodynamics from phonon and Debye model: application to Ni and Ni₃Al, *Comput. Mater. Sci.* 47 (2010) 1040–1048, <https://doi.org/10.1016/j.commatsci.2009.12.006>.
- [37] U. Häussermann, S.I. Simak, I.A. Abrikosov, B. Johansson, S. Lidin, Electronically induced phase transitions in ternary transition metal distannide systems, *J. Am. Chem. Soc.* 120 (1998) 10136–10146, <https://doi.org/10.1021/ja981347t>.
- [38] W.L. Neijmeijer, B.H. Kolster, The ternary system Nb–Sn–Cu at 675 °C, *Z. Metallkd.* 78 (1987) 730–737, <https://doi.org/10.1515/ijmr-1987-781009>.
- [39] V. Pan, V. Latysheva, Y. Litvinenko, V. Flis, V. Gorskiy, Phase equilibria and superconducting properties of Nb–Sn–Cu alloys, *Phys. Met. Metallogr.* 49 (1980) 170–173.
- [40] V.V. Baron, E.I. Gladishvskii, A.R. Kadirbaev, R.B. Skolozdra, Structure and superconducting properties of Nb–Sn–Cu alloys, *Sverchprovodjascie Mater.* (1983) 53–56.
- [41] U. Zwicker, L. Rinderer, Untersuchungen zur Bildung der Nb₃Sn-A15-Phase bei Temperaturen unter 800 °C, *Z. Metallkd.* 66 (1975) 738–748, <https://doi.org/10.1515/ijmr-1975-661208>.
- [42] R.H. Hopkins, G.W. Roland, M.R. Daniel, Phase relations and diffusion layer formation in the systems Cu–Nb–Sn and Cu–Nb–Ge, *Metall. Trans. A* 8A (1977) 91–97.
- [43] N.V. Ageeva, Cu–Nb–Sn, Diagrammy Sostoyaniya Metallicheskih Sistem 2, 1982, p. 26.
- [44] I. Dietrich, G. Lefranc, A. Müller, Abschirmverhalten von Niob-Zinn-Sintermaterial bei Zugabe von Fremdelementen, *J. Less Common. Met.* 29 (1972) 121–132.
- [45] H. Yamasaki, Y. Kimura, Fabrication of Nb₃Sn superconductors by the solid-liquid diffusion method using Sn rich CuSn alloy, *Cryogenics* 22 (1982) 89–93, [https://doi.org/10.1016/0011-2275\(82\)90100-X](https://doi.org/10.1016/0011-2275(82)90100-X).
- [46] C. Toffolon, C. Servant, J.C. Gachon, B. Sundman, Reassessment of the Nb–Sn system, *J. Phase Equil.* 23 (2002) 134–139.
- [47] D. Li, P. Franke, S. Fürtauer, D. Cupid, H. Flandorfer, The Cu–Sn phase diagram part II: new thermodynamic assessment, *Intermetallics* 34 (2013) 148–158, <https://doi.org/10.1016/j.intermet.2012.10.010>.
- [48] C. Wieser, W. Hügel, A. Walnsch, A. Leineweber, Two-phase η' + η region in Cu₆Sn₅ intermetallic: insight into the order–disorder transition from diffusion couples, *J. Electron. Mater.* 49 (2020) 245–256, <https://doi.org/10.1007/s11664-019-07643-3>.
- [49] A. Matsakova, B.G. Lazarev, Peculiarities of the constitutional phase diagram of the system Nb–Sn, *Phys. Met. Metallogr.* 35 (1973) 133–141.
- [50] Z.-K. Liu, J. Ågren, Morphology of cementite decomposition in an Fe–Cr–C alloy, *Metall. Trans. A* 22 (1991) 1753–1759, <https://doi.org/10.1007/BF02646499>.
- [51] Z.-K. Liu, L. Höglund, B. Jönsson, J. Ågren, An experimental and theoretical study of cementite dissolution in an Fe–Cr–C alloy, *Metall. Trans. A* 22 (1991) 1745–1752, <https://doi.org/10.1007/BF02646498>.
- [52] E.-A. Zen, Validity of “Vegard’s law”, *Am. Mineral.* 41 (1956) 523–524.
- [53] A. Leineweber, S.L. Shang, Z.K. Liu, C-vacancy concentration in cementite, Fe₃C_{1-z}, in equilibrium with α-Fe[C] and γ-Fe[C], *Acta Mater.* 86 (2015) 374–384, <https://doi.org/10.1016/j.actamat.2014.11.046>.

- [54] J. Hafner, Ab-initio simulations of materials using VASP: density-functional theory and beyond, *J. Comput. Chem.* 29 (2008) 2044–2078, <https://doi.org/10.1002/jcc.21057>.
- [55] A.T. Dinsdale, *SGTE Pure Element (Unary) Database, Version 5.0, 2009*.
- [56] M. Hillert, The compound energy formalism, *J. Alloys Compd.* 320 (2001) 161–176, [https://doi.org/10.1016/S0925-8388\(00\)01481-X](https://doi.org/10.1016/S0925-8388(00)01481-X).
- [57] O. Redlich, A.T. Kister, Algebraic representation of thermodynamic properties and the classification of solutions, *Ind. Eng. Chem.* 40 (1948) 345–348, <https://doi.org/10.1021/ie50458a036>.
- [58] J.-O. Andersson, T. Helander, L. Höglund, P. Shi, B. Sundman, Thermo-Calc & DICTRA, computational tools for materials science, *Calphad* 26 (2002) 273–312, [https://doi.org/10.1016/S0364-5916\(02\)00037-8](https://doi.org/10.1016/S0364-5916(02)00037-8).
- [59] T.B. Massalski, H.W. King, Alloy phases of the noble metals, *Prog. Mater. Sci.* 10 (1963) 3–78, [https://doi.org/10.1016/0079-6425\(63\)90008-2](https://doi.org/10.1016/0079-6425(63)90008-2).
- [60] E. Scheil, Darstellung von Dreistoffsystemen, *Arch. für das Eisenhüttenwes.* 9 (1936) 571–573, <https://doi.org/10.1002/srin.193600784>.